Electrochimica Acta 186 (2015) 201–208

Contents lists available at ScienceDirect

Electrochimica Acta

journal homepage: www.elsevier.com/locate/electacta

Synergistic effects of coating and doping for lithium ion battery cathode materials: synthesis and characterization of lithium titanate-coated $LiCoO_2$ with Mg doping

Jae-Hyun Shim[a], Jaehan Lee[a], Sang Yun Han[b], Sanghun Lee[c,*]

[a] Battery R&D Center, Samsung SDI Co. Ltd., Suwon, Gyunggido, 443-803, Republic of Korea
[b] Department of Nanochemistry, Gachon University, Gyunggido, 461-701, Republic of Korea
[c] Department of BioNano Technology, Gachon University, Gyunggido, 461-701, Republic of Korea

ARTICLE INFO

Article history:
Received 8 June 2015
Received in revised form 8 October 2015
Accepted 23 October 2015
Available online 11 November 2015

Keywords:
lithium ion battery
lithium titanate
synergistic effect
lithium cobalt oxide

ABSTRACT

Lithium titanates are introduced as coating materials on the surface of Mg-doped $LiCoO_2$ in which the residual Li_2CO_3 after synthesis of the active materials is used as a lithium source. It is revealed that two completely different lithium titanate phases (monoclinic Li_2TiO_3 and spinel $Li_4Ti_5O_{12}$) can be obtained as the coating materials depending on the concentration of a titanium source. Characterization of the coating materials is performed with various experimental techniques including XRD, nano SIMS, TEM, EELS and current measurement using nano probe. The $Li_4Ti_5O_{12}$ coating layer from the high concentration of titanium source secures better electrochemical performances than the Li_2TiO_3 one from the low concentration of titanium source due to its "zero-strain" characteristic. In addition, it is shown that the doped ions (Mg^{2+}) from the active materials move to the coating layer and strongly enhance the conductivity of $Li_4Ti_5O_{12}$. Consequently, synergistic effects on the cell performances of cyclability and rate capability from coating and doping for the $LiCoO_2$ cathode materials are rigorously investigated.

© 2015 Elsevier Ltd. All rights reserved.

1. Introduction

Since the first commercialization of lithium ion battery (LIB), the layered lithium transition metal oxides ($LiMO_2$, M: Co, Ni, Mn, and so forth) have been one of the most predominant cathode materials in LIBs, particularly, for portable electronics. However, as the usage of LIBs has increased in other area, such as, transport applications (electric vehicles and hybrid electric vehicles) and massive energy storage facilities, demands for better electrochemical performances of LIBs are drastically increasing. From various experimental evidences, several degradation mechanisms of the layered cathode materials have been proposed [1–4]. One is the dissolution of transition metal ions into the electrolytes when the electrode is delithiated. Another mechanism is that the MO_2 layer at the delithiated state shears from the electrode surface, which results in the capacity fade. In addition, the mechanically vulnerable charged form of the materials with the expanded lattice suffers from oxygen loss and side reaction with electrolytes at the highly oxidized surfaces. None of these mechanisms are mutually exclusive, and conceivably multiple mechanisms are concurrently involved in a cathode degradation.

Coating is one of the simplest as well as most effective methods to be considered for minimization of the degradation and consequent capacity fade during cycling. The primary role of the coating layer is physical protection from chemical reaction with the electrolytes. The common feature of successful coating materials, such as, ZrO_2, SiO_2, ZnO, Al_2O_3, $Al(OH)_3$, $AlPO_4$, and AlF_3, is that the metal ion in the coating layer has only one stable valence state at ambient condition [5], therefore, the active materials can obtain much enhanced stability. However, because the coating materials generally exhibit poor lithium ion conduction, recently, inorganic materials containing lithium ions have been proposed. For example, Lu et al. suggested that monoclinic Li_2TiO_3, a Li-rich layered material similar to Li_2MnO_3, would be a good candidate [6]. They showed that the Li_2TiO_3-coated $LiMO_2$ nanobelts strongly improved rate capability and cycling ability as cathode materials. The effect of Li_2TiO_3 is not limited only to the layered materials. Deng et al. reported that this material worked well for the $LiNi_{0.5}Mn_{1.5}O_4$ spinel cathode [7]. They showed that the Li_2TiO_3-coated samples delivered excellent discharge capacities even at a very high charging/discharging rate of 5C. Meanwhile, $Li_4Ti_5O_{12}$ is another example of lithium ion conductor

* Corresponding author.
E-mail address: sanghunlee@gachon.ac.kr (S. Lee).

http://dx.doi.org/10.1016/j.electacta.2015.10.135
0013-4686/© 2015 Elsevier Ltd. All rights reserved.

being used as a coating material. In fact, it has been extensively used as an anode material for a long time because it rarely suffers from volume change, which is so called a "zero-strain" material, during ion insertion and extraction [8–10]. However, because $Li_4Ti_5O_{12}$ shares the same structure of spinel ($Fd\overline{3}m$) with $LiMn_2O_4$ and the crystallographic mismatch between them (lattice parameter a of $Li_4Ti_5O_{12}$: 8.248 Å and that of $LiMn_2O_4$: 8.357 Å) is not significant, $Li_4Ti_5O_{12}$ or its similar derivatives have been suggested as a coating material on the spinel cathodes [11–14]. Meanwhile, even though a few studies reported that $Li_4Ti_5O_{12}$ can be applied to the layered materials, for example, $LiCoO_2$ [15–18], it has not been so successful in industry, probably because it does not produce acceptable electrochemical performances, such as, cycling lifetime and high rate capability. This disqualification is mainly ascribed to its low electrical conductivity ($\sigma < 10^{-13}$ S cm^{-1}) [19].

By modifying electronic structure of original active materials, doping is a simple method to efficiently improve cell performances. For example, because Mg has a valence state of 2^+ rather than Co (3^+) or Li (1^+), the Mg-doped $LiCoO_2$ exhibits strong electrical conductivity compared to the bare $LiCoO_2$ and, therefore, it shows excellent cell performances [20–24]. Besides Mg, various dopants for $LiCoO_2$, such as, Al [25], Zr [26], Sn [27], B [28], and so forth [29], have also been explored. In this study, with combination of the above-mentioned coating of lithium titanate and doping of Mg, we investigate their synergistic effects on the $LiCoO_2$ cathode materials. From various experimental works including X-ray diffraction (XRD), nano secondary ion mass spectrometry (nano SIMS), transmission electron microscopy (TEM), electron energy-loss spectroscopy (EELS), current measurement by nano probe, and electrochemical characterization, it is revealed that the doped ions (Mg^{2+}) have an effect not only on the active materials themselves but also on the coating layer. In addition, utilizing limited amounts of residual lithium ions, it is shown that the phase of lithium titanate is varied with the contents of Ti source. Because the phases are very different in several respects, the electrochemical performances of the cells employing them are also consequently different.

2. Experimental Section

2.1. Synthesis of materials

The Mg-doped $LiCoO_2$ ($LiMg_{0.01}Co_{0.99}O_2$) was prepared by solid-state reaction. Starting materials of Li_2CO_3, Co_3O_4 and Mg $(CO_3)_4$•$Mg(OH)_2$•$5H_2O$ were mixed by a mechanical mixer with a rotating speed of 80 rpm for 1 h. The ratio of Li: Co: Mg was adjusted to 1.04: 0.99: 0.01 considering that unreacted Li_2CO_3 remains on the surface of Mg-doped $LiCoO_2$ particles after synthesis. Then, the powder mixtures were heated at 1000 °C for 5 h in air to produce the Mg-doped $LiCoO_2$. The sol-gel technique was employed for the lithium titanate coating. For this purpose, various amounts of $Ti(OBu)_4$ (0.457 g, 1.372 g, and 2.286 g) were, respectively, dissolved in 100 g of ethanol with 3 h stirring at room temperature. Then, 50 g of the synthesized active materials was added into each of the solutions with 4 h stirring at 80 °C. The residual Li_2CO_3 on the surface of the active materials was used as a lithium source for the coating. Utilization of the residual Li_2CO_3 has a benefit because impurities such as LiOH or Li_2CO_3 usually impede the Li ion diffusion and charge transfer reactions at the interfaces and promote the formation of HF [30]. Moreover, Li_2CO_3 has been considered as a main source of CO_2 gas at high temperatures. Then, each of the solutions was heated at 950 °C for 6 h and then naturally cooled down to room temperature. As described in Scheme 1, the structure of lithium titnate coating layer is

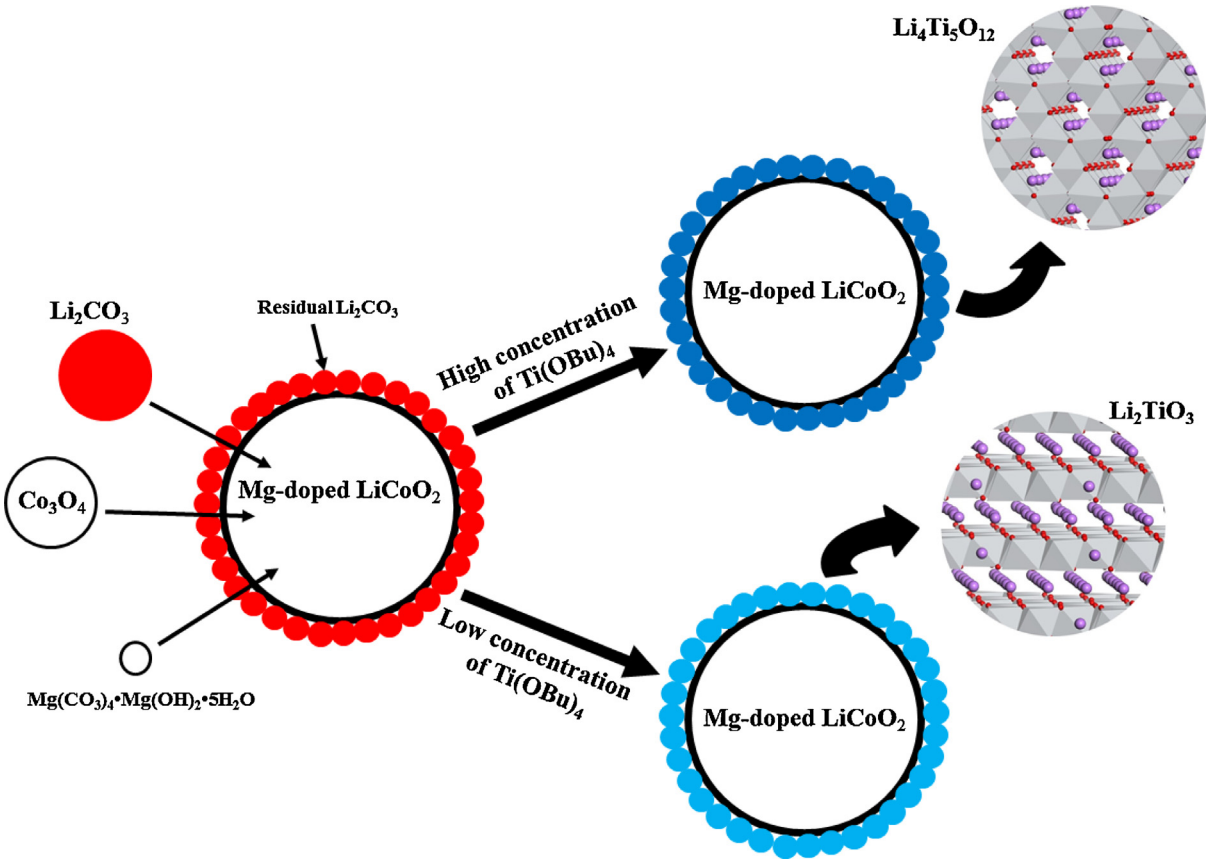

Scheme 1. Synthesis and Coating Process of Lithium Titanate-Coated $LiCoO_2$.

dependent on the concentration of Ti source, which will be thoroughly examined and discussed in the section of Results and Discussion. For comparison, uncoated but Mg-doped $LiCoO_2$ and lithium titanate-coated with high concentration of $Ti(OBu)_4$ (2.230 g in ethanol 100 g) but Mg-undoped $LiCoO_2$ were also prepared through similar processes. The denotation of each material is summarized in Table 1.

2.2. Characterization of materials

To study structures of the materials, XRD measurements were employed using a Philips X'PERT PRO diffractometer with Cu Kα radiation. Diffraction patterns were obtained for $2\theta = 10^\circ \sim 130^\circ$ with step size of 0.013° and scan rate of 0.67°/min. Silicon powder (Aldrich, 99 %) was used as an internal standard to calculate cell parameters. The spatial distributions of elements on the cross section of the particles were analyzed by nano SIMS (Cameca Nano-SIMS 50, France), the resolution of which was 50 nm. The data were obtained in multi-collection detector mode by sputtering the sample with a ~0.4 pA Cs primary ion beam (impact energy: 16 keV) focused to a spot of ~100 nm diameter. The primary ion beam was rastered over $15 \times 15\ \mu m^2$. The samples were mounted using epoxy resin and then polished with SiC paper. In the negative mode, the detected ions were $^{7}Li^{16}O^-$, $^{24}Mg^{16}O^-$, $^{48}Ti^{16}O^-$, and $^{59}Co^{16}O^-$. The scanning TEM (STEM) observations were performed using a Cs-corrected STEM (JEM-2100F, JEOL Co., Japan) at 200 kV, which is equipped with a spherical aberration corrector (CEOS Gmbh, Germany) at the Korea Advanced Nano Fab Center (KANC). The size of minimum probe is ~1 Å in diameter. The samples for the STEM measurements were prepared by Focused Ion Beam (FIB, Hellios FEI, USA). The EELS was performed using a spectrum-image scheme based on the STEM observation (Gatan GIF 200 spectrometer). The energy resolution estimated by the full width at half maximum of the zero loss peaks was about 0.8 eV and the energy dispersion was 0.05 eV/ch. The current-voltage characteristics of the active materials and the lithium titanate coating layers were measured by nano probe (Nanostation, KLEINDIEK, Germany) with a scanning electron microscope (SEM). To acquire the current-voltage curves, the voltage was applied from -4 V to 4 V.

2.3. Measurement of electrochemical performances

To study the electrochemical performances, 2032 coin-type cells were prepared. First, the active materials, conducting materials (Super-P carbon black) and binders (polyvinylidene fluoride) were blended with a ratio of 96: 2:2 (in wt%) in N-methyl-2-pyrrolidone. Then, the slurry was cast on aluminum foil and dried at 110 °C for 10 h in a vacuum oven. The electrolyte for the cells was 1.15 M $LiPF_6$ in ethylene carbonate/diethyl carbonate/ethyl methyl carbonate (30: 30: 40 in vol%) + fluoroethylene carbonate 5% (Panax etec Co., Ltd, Korea). The lithium foil was used as the negative electrode and the capacity of the manufactured cells was 1.5 mAh/cm^2. The reversible discharge capacities were measured between 3.0 and 4.5 V. The AC-impedance measurements were performed using a Biologic VMP3 impedance analyzer over the frequency range of 500 kHz ~5 mHz with amplitude of 10 mV.

Table 1
Notation of the Materials in This Study.

Name	Amount of $Ti(OBu)_4$ for lithium titanate coating (g/100 g of ethanol)	Mg doping (Co: Mg = 0.99: 0.01)
LT0-LCO_{Mg}	0.457	O
LT1-LCO_{Mg}	1.372	O
LT2-LCO_{Mg}	2.286	O
Uncoated-LCO_{Mg}	None	O
LT2-LCO	2.230	X

3. Results and Discussion

Fig. 1 shows lattice parameters of the samples obtained from the Rietveld refinement of the XRD data. Compared to the pristine (undoped) $LiCoO_2$, the Mg-doped ones including uncoated-LCO_{Mg}, LT0-LCO_{Mg}, LT1-LCO_{Mg}, and LT2-LCO_{Mg} have larger *a* and *c* parameters, which is caused by larger ionic size of Mg^{2+} (0.72 Å) than Co^{3+} (0.545 Å). This observation is consistent with the previous studies [22,26,31]. Interestingly, the lattice parameters are slightly reduced with lithium titanate coating. This indicates that the concentration of Mg^{2+} ions in the active materials has decreased when they are coated with lithium titanates, in other words, a small amount of Mg^{2+} ions in the Mg-doped $LiCoO_2$ has diffused to the coating layer. This migration of Mg^{2+} ions is clearly evidenced by nano SIMS analysis. As shown in Fig. 2, the Mg^{2+} ions are homogeneously distributed over the entire particle of uncoated-LCO_{Mg} whereas the Mg map of the LT2-LCO_{Mg} particle exhibits slightly larger population at the edges of particle (yellow arrows) than in the bulk (inner area), which is in accord with the Ti map even though its intensity is much smaller. A few studies have reported that metal ions from coating layer, for example, MgO, diffuse into the interlayers of $LiCoO_2$ active materials during electrochemical processes, and advance the cell performances [32–34], however, the diffusion in the reverse direction (from active materials to coating layer) either before or during electrochemical processes has never been noted previously. The diffused Mg^{2+} ions enhance a role of the coating layer to improve electrochemical performances, which will be discussed in the later part. Thickness of the coating layer is too thin (~200 nm) to characterize its detailed structure by XRD (Fig. S1 in Supplementary Data).

In order to characterize the structural features of the cathode materials in the nm scale, a spherical aberration-corrected STEM was employed. The contrast of the high-angle annular-dark-field (HAADF) image shows the $Z^{1.7}$ dependency, instead of $Z^{1/3}$ for annular-bright-field (ABF) image, where Z is the atomic number [35]. Fig. 3 shows HAADF STEM images of lithium titanate-coated and Mg-doped $LiCoO_2$ with different coating levels. LT0-LCO_{Mg}, that is, the sample coated by the low concentration of $Ti(OBu)_4$ seems to be divided into two regions (L and M in Fig. 3a) with respect to their contrast. From the fast Fourier transform (FFT)

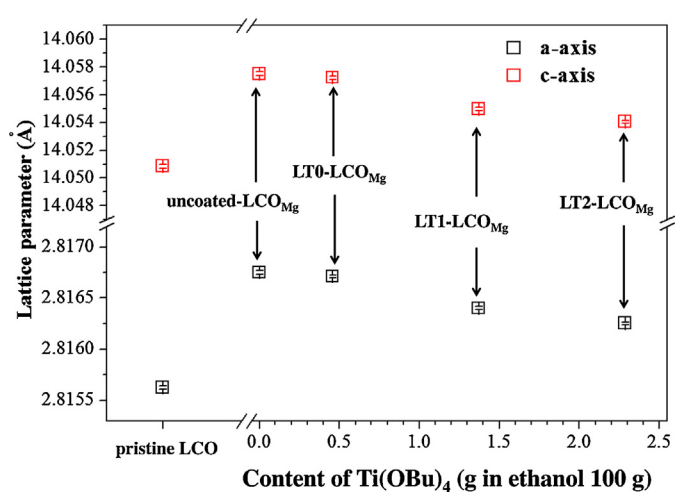

Fig. 1. Lattice parameter vs content of $Ti(OBu)_4$ for $LiCoO_2$.

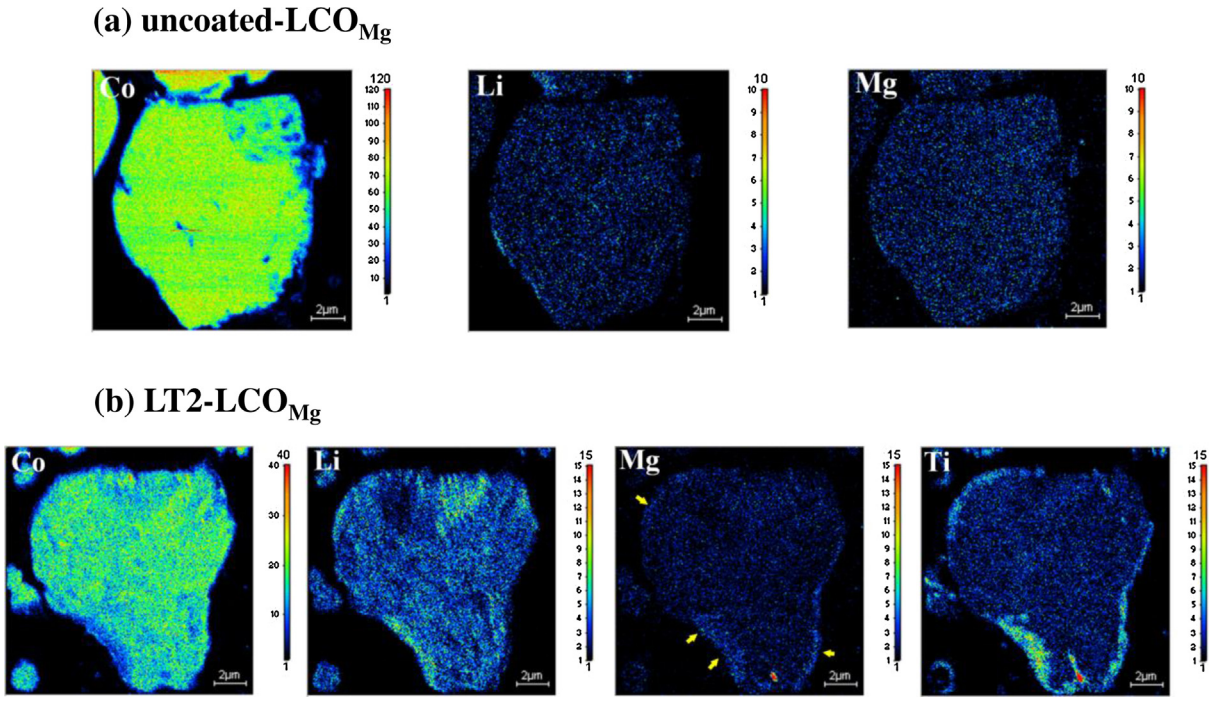

Fig. 2. Elemental distributions of metals on the cross sections of (a) uncoated-LCO$_{Mg}$ and (b) LT2-LCO$_{Mg}$ particles obtained by nano SIMS. (For interpretation of the references to color in text, the reader is referred to the web version of this article.)

patterns, regions L and M were identified as $LiCoO_2$ ($R\bar{3}m$) and Li_2TiO_3 ($C2/c$), respectively. It is noteworthy that the Li_2TiO_3 crystal was epitaxially grown on the surface of $LiCoO_2$ as a coating layer. The [0 0 1] direction of $LiCoO_2$ (c-axis) was completely parallel to the [0 0 1] direction of Li_2TiO_3. Meanwhile, LT2-LCO$_{Mg}$, that is, the sample coated by the high concentration of $Ti(OBu)_4$ is also divided into two regions (L and N in Fig. 3c), however, the structure of coating layer (region N) is distinct from that of LT0-LCO$_{Mg}$. From the FFT analysis, it was determined as the spinel structure of $Li_4Ti_5O_{12}$ ($Fd\bar{3}m$). In more detail, the enlarged STEM image inserted in region N shows that the lattice spacing is ~0.48 nm, which is corresponding to that of the (111) or ($1\bar{1}\bar{1}$) planes of spinel $Li_4Ti_5O_{12}$. For LT1-LCO$_{Mg}$, that is, the sample coated by the moderate concentration of $Ti(OBu)_4$, differently with the previous cases, three discriminable regions (L, M, and N) are shown in the STEM image (Fig. 3b). In this case, from the FFT analysis, it was revealed that the monoclinic Li_2TiO_3 phase is grown on the $LiCoO_2$ surface, and then, the spinel phase of $Li_4Ti_5O_{12}$ is developed on top of the monoclinic one. This dependence of coating layer structure on the concentration of Ti source is caused by the ratio of Li and Ti for the stable states of lithium titanates. According to the phase diagram of Li_2O-TiO_2 binary system [36], $Li_4Ti_5O_{12}$ is the stable phase under the condition of more than 71 mol% of TiO_2 whereas Li_2TiO_3 is the stable one when TiO_2 is less than 51 mol%. Between the two concentration limits, solid solutions of $Li_4Ti_5O_{12}$ and Li_2TiO_3 are favored. In our study, only the contents of Ti source are varied while those of Li source (residual lithium on the surface of $LiCoO_2$ particles) are fixed, therefore, it is considered that the structural variation of the coating layer in this work complies with the phase diagram. Additional TEM images and diffraction patterns from different zone-axes are included in Supplementary Data to clearly distinguish the structures (Fig. S2).

To evaluate the electrochemical performances of lithium titanate-coated and Mg-doped $LiCoO_2$ (LT0-LCO$_{Mg}$, LT1-LCO$_{Mg}$,

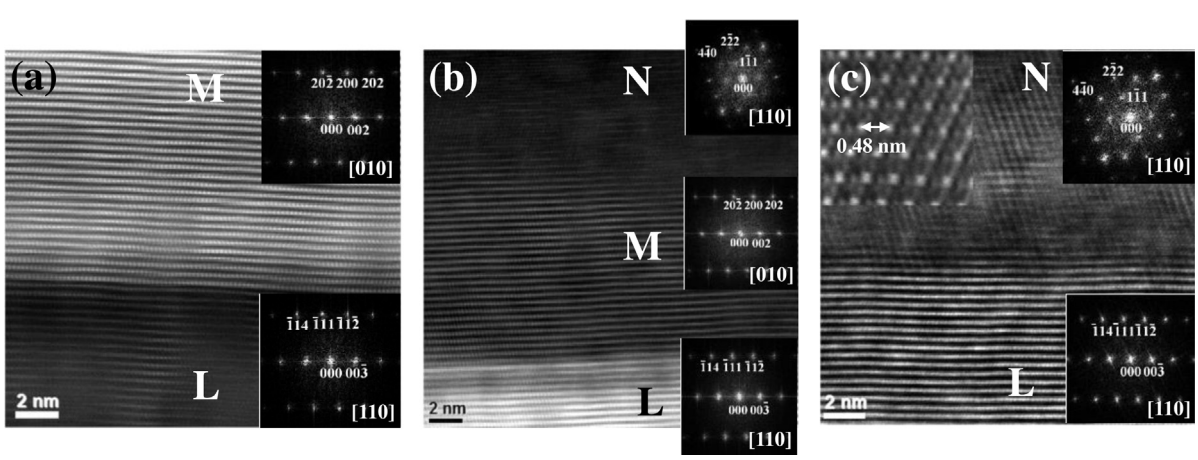

Fig. 3. HAADF STEM images of (a) LT0-LCO$_{Mg}$, (b) LT1-LCO$_{Mg}$, and (c) LT2-LCO$_{Mg}$. The insets on right side of each image are the FFT patterns of corresponding regions. The inset on left side of (c) is enlarged image of region N.

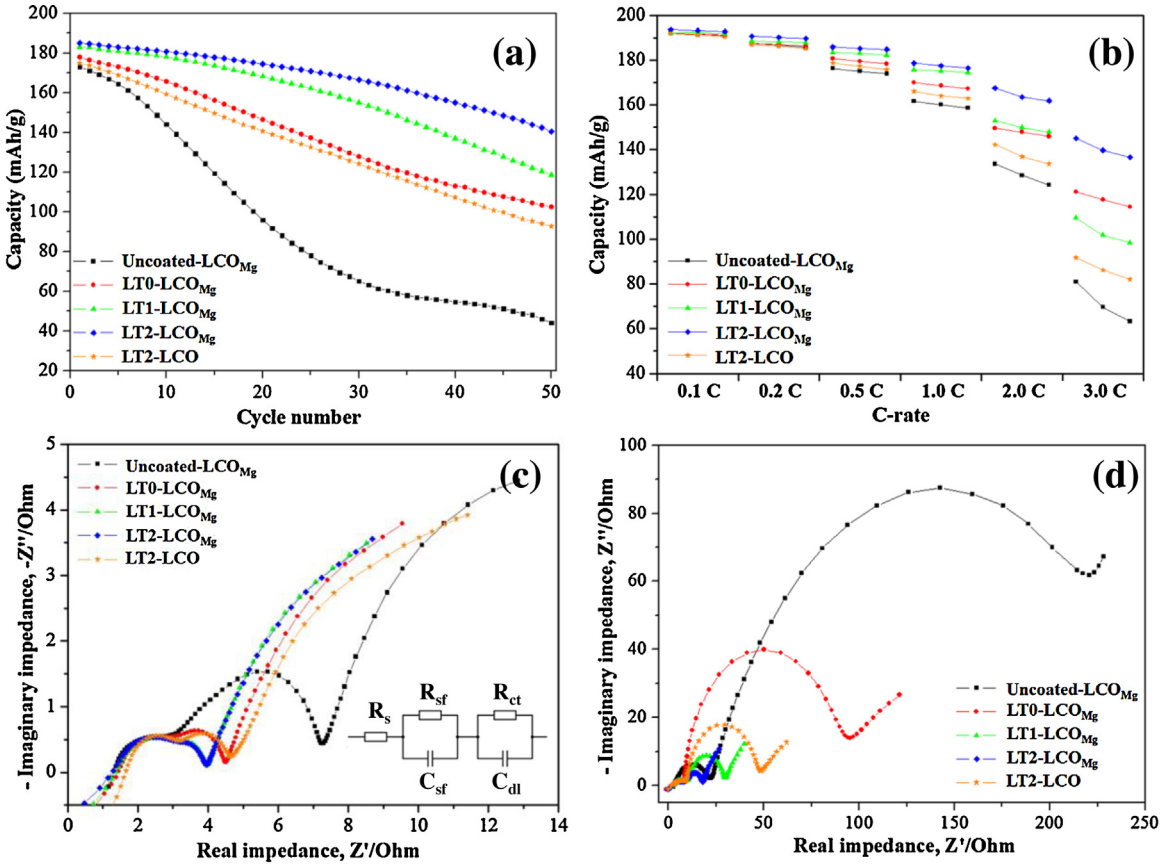

Fig. 4. Cycling performances of various cathode materials with different coatings measured at (a) 1C-rate and (b) incremental charging/discharging rates from 0.1C to 3C in the range of 3.0-4.5 V. Nyquist plots measured at (c) 2nd and (d) 50th cycle. The inset diagram in (c) is an equivalent circuit. (R_s, R_{sf}, and R_{ct} are the resistances of electrolyte solution, solid electrolyte interface, and charge transfer at the interface of cathode/electrolyte, respectively. C_{sf} and C_{dl} are the capacitances of solid electrolyte and double layer, respectively.)

and LT2-LCO$_{Mg}$), 2032 coin-type cells were assembled with Li metal as an anode. For comparison, uncoated-LCO$_{Mg}$ and LT2-LCO (without Mg doping) were also tested. The cycling abilities at a rate of 0.5C (=160 mAh/g) are compared in Fig. 4a, where the capacities were measured within a range of 3.0–4.5 V. LT2-LCO$_{Mg}$ exhibits not only the highest discharge capacity at the first cycle (184.9 mAh/g) but also the best capacity retention of higher than 76% after 50 cycles (140.6 mAh/g). Compared to uncoated-LCO$_{Mg}$ (172.2 mAh/g), the improvement in the initial capacity of LT2-LCO$_{Mg}$ is considerable (higher by 7%). However, even more remarkable is the enhancement in the cycling ability. After 50 cycles, the capacity retention of uncoated-LCO$_{Mg}$ is just 25% (44.0 mAh/g) of the initial capacity. Even though somewhat advancement of the electrochemical performances is also managed by the coatings with low or moderate concentrations of Ti source, the significance is not so much as LT2-LCO$_{Mg}$. Therefore, it is considered that the coating layer of LT2-LCO$_{Mg}$ (spinel $Li_4Ti_5O_{12}$) provides better performances for $LiCoO_2$ cathode than that of LT0-LCO$_{Mg}$ (monoclinic Li_2TiO_3). In fact, this discrepancy in effectiveness of the coatings comes not only from the volume (or area) of the coating layer but also from the structural or phase stability during cycling, which will be shown and discussed further in the later part. In addition, Mg doping assists in improving the cell performances. As shown in Fig. 4a, the coating effect without the Mg doping is fairly limited, which is probably related to the low electronic conductivity of the coating materials. Fig. 4b shows a cycling result at incremental charging/discharging rates from 0.1C to 3C. At 0.1C, the discharge capacities of the samples are almost the same, however, at the high C-rates, the capacity of LT2-LCO$_{Mg}$ is strongly improved compared to that of uncoated-LCO$_{Mg}$. In this rate capability experiment, a synergistic effect of coating and doping is observed as well. We obtained useful information of charge transfer property from electrochemical impedance spectroscopy (EIS) measurements. In Fig. 4c and d, the Nyquist plots of the cells from the differently treated cathode materials at the 2nd and the 50th cycle are compared. An equivalent circuit is presented in the figure inset. The intercept at real impedance (Z') axis at the high frequency corresponds to the solution resistance (R_s), which is the impedance related to ion diffusion in the electrolyte solution. The high and low frequency semicircles are attributed to the solid electrolyte interface resistance (R_{sf}) and the charge transfer resistance at the interface of cathode/electrolyte (R_{ct}), respectively. All the impedance components (R_s, R_{sf}, and R_{ct}) are listed in Table 2. At the 2nd cycle, LT2-LCO$_{Mg}$ shows the smallest resistances, but the differences are insignificant. Meanwhile, at the 50th cycle, all the resistances become large as a result of cycling degradation. In particular, R_{ct} is most significantly increased, which means that the charge transfer at the interface of cathode/electrode becomes hard

Table 2
Resistances Obtained from Equivalent Circuit Fitting of EIS Experimental Data.

Samples	2nd cycle			50th cycle		
	R_s (Ω)	R_{sf} (Ω)	R_{ct} (Ω)	R_s (Ω)	R_{sf} (Ω)	R_{ct} (Ω)
Uncoated-LCO$_{Mg}$	1.33	5.23	16.21	3.00	19.58	247.0
LT0-LCO$_{Mg}$	1.43	3.74	11.79	1.45	7.46	89.38
LT1-LCO$_{Mg}$	1.41	2.65	11.66	2.00	7.30	22.60
LT2-LCO$_{Mg}$	1.27	2.56	10.99	2.20	6.69	9.98
LT2-LCO	1.66	3.12	12.05	1.92	7.80	41.36

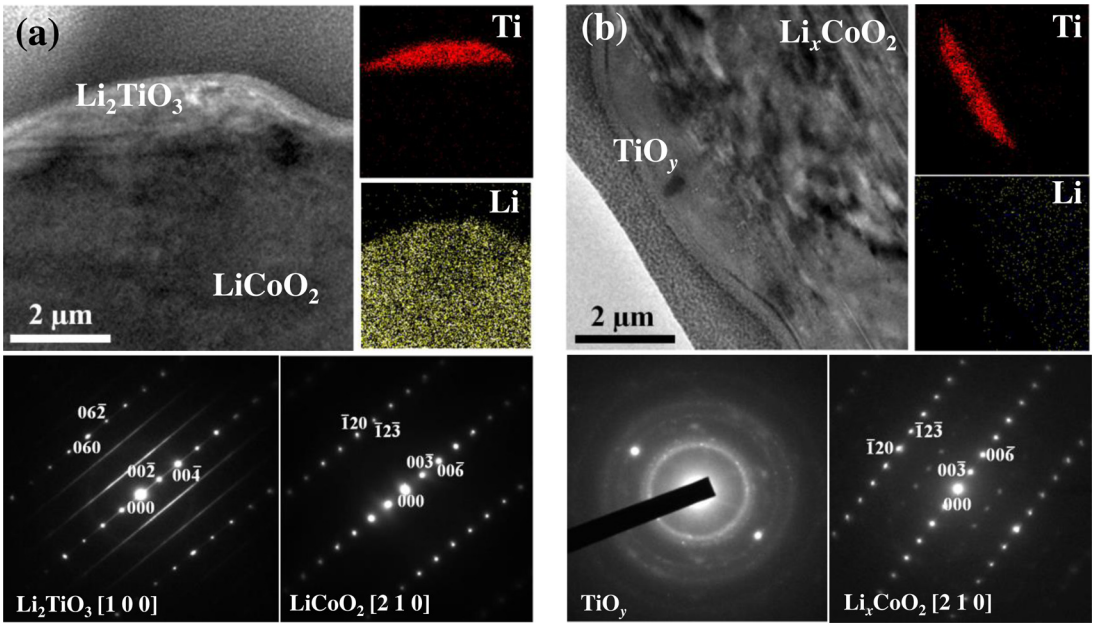

Fig. 5. Bright-field TEM images (main figures), SAED patterns of coating layers (bottom left figures) and active materials (bottom right figures), and Ti/Li maps from EELS (right figures) of (a) fresh (uncycled) and (b) first-charged state of LT0-LCO_{Mg}.

to occur. The smaller R_{ct} of LT2-LCO_{Mg} than LT0-LCO_{Mg} is in agreement with the experimental results of lithium conductivities of $Li_4Ti_5O_{12}$ [37] and Li_2TiO_3 [38]. The relatively high ionic conductivity of $Li_4Ti_5O_{12}$ possibly alleviates the cycling deterioration and consequential rapid rise of R_{ct}.

In order to trace an origin of the different effectiveness of monoclinic Li_2TiO_3 and spinel $Li_4Ti_5O_{12}$ as coating materials, the structural changes of the materials after charging (delithiating) were investigated by TEM. Fig. 5a shows a TEM image, selected area electron diffraction (SAED) patterns, and EELS maps of Ti and Li of fresh (uncycled) LT0-LCO_{Mg}. The electron incidence was along the [1 0 0] zone-axis of Li_2TiO_3, which is parallel to [2 1 0] zone-axis of $LiCoO_2$. The typical diffraction spots of monoclinic phase of Li_2TiO_3 and hexagonal phase of $LiCoO_2$ are respectively observed in their SAED patterns. It has been known that the lines between the main reflections of the Li_2TiO_3 phase are from the stacking faults of $LiTi_2$ metal layers [39]. Meanwhile, Fig. 5b exhibits the same analysis of LT0-LCO_{Mg} after the first charge. For the $LiCoO_2$ phase, in addition to the original diffraction spots of the hexagonal phase, weak but new diffraction spots are appeared in the middle of them. The additional spots are attributed to the characteristics of the charged (partially delithiated) state of lithium cobalt oxide (LixCoO2). As shown in the EELS maps, the Li ions in the Li_2TiO_3 coating layer are completely extracted after charging, which means that they are electrochemically active in the range of operating voltages, while the Ti ions still remain in that layer. The SAED pattern of the TiO_y layer shows diffused diffraction rings, which indicates that a substantial amount of the delithiated coating layer loses its

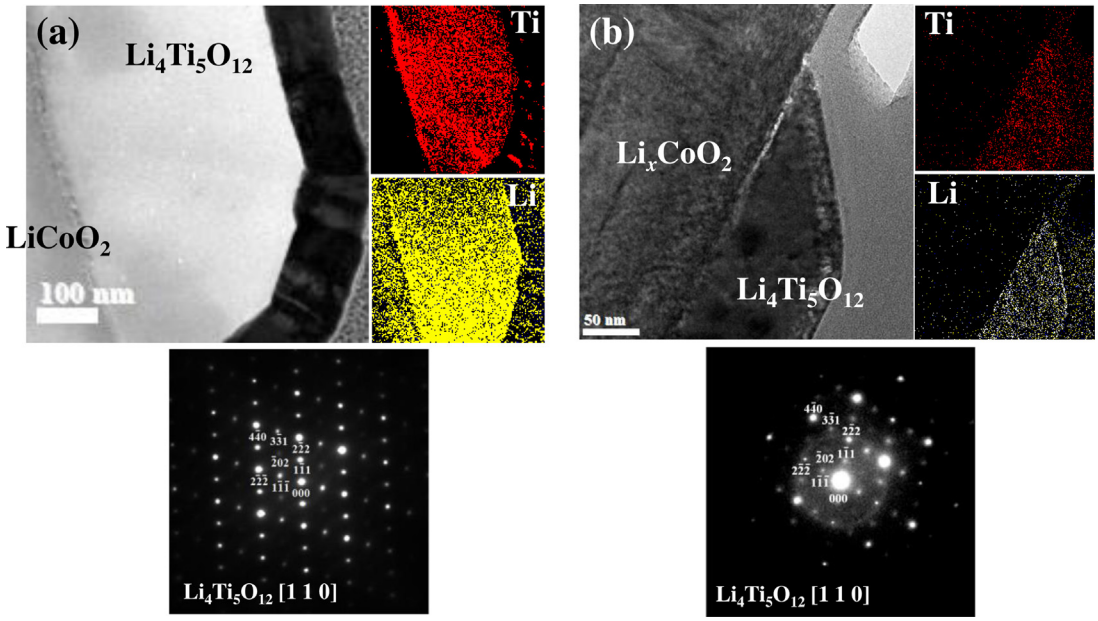

Fig. 6. Bright-field TEM images (main figures), SAED patterns of coating layer (bottom figures), and Ti/Li maps from EELS (right figures) of (a) fresh (uncycled) and (b) first-charged state of LT2-LCO_{Mg}. The SAED patterns of active materials are the same as those of LT0-LCO_{Mg} in Fig. 5.

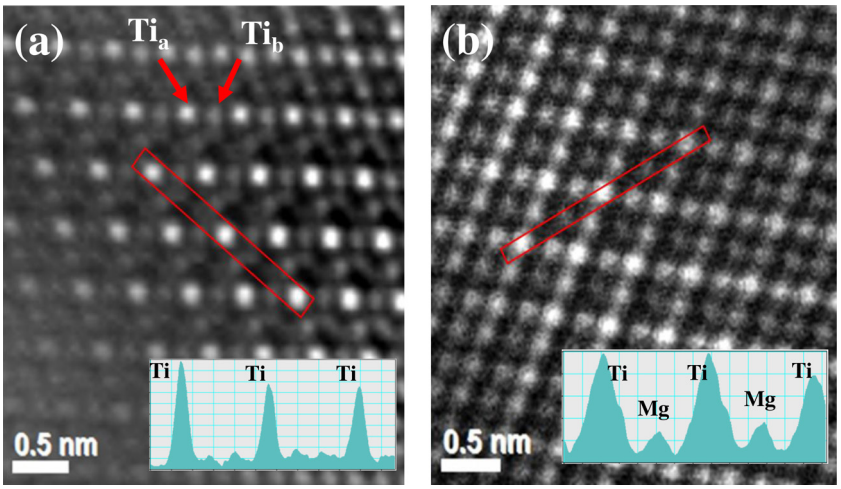

Fig. 7. HAADF STEM images of first charged state of (a) (undoped) LT2-LCO and (b) LT2-LCO$_{Mg}$. The insets are the contrast line profiles in red rectangles. For explanation of Ti$_a$ and Ti$_b$ with different brightness in (a), see the text.

monoclinic crystalline structure. The same analysis was done on LT2-LCO$_{Mg}$ (Fig. 6). The EELS map of Li shows that Li ions in $Li_4Ti_5O_{12}$ do not leave from the coating layer during the first charge while the majority of Li ions in $LiCoO_2$ are extracted. In addition, the SAED pattern of $Li_4Ti_5O_{12}$ phase, in which the electron incidence was along with [1 1 0] zone-axis, after the first charge is almost the same as that of the fresh sample except the diffraction spots in the former become slightly more diffused than those in the latter. This observation indicates that the $Li_4Ti_5O_{12}$ coating layer still maintain the crystalline structure after charge, that is, the "zero strain" characteristic, unlike the Li_2TiO_3 coating layer. In conclusion, the most crucial difference between the two coating layers is the electrochemical activity of the Li ions that they carry inside themselves. If the Li ion cycling of a material is sufficiently reversible, the electrochemical activity itself might not be a matter. However, the lithiation/delithiation of Li_2TiO_3 is catastrophically irreversible, therefore, the coating layer of Li_2TiO_3 phase possibly acts as a resistance after some cycling (large R_{ct}) as shown by the EIS experiment. This is reminiscent of the relatively poor cyclability of layered-layered composite cathode materials, one component of which is lithium-rich metal oxide, for example, Li_2MnO_3 [40]. TEM images and SAED patterns obtained after 50 cycles (Fig. S3 in Supplementary Data) demonstrate the irreversible transformation of Li_2TiO_3 and the structure consistency of $Li_4Ti_5O_{12}$ with cycling.

In order to study the synergistic effects of coating and doping for the cathode materials, the $Li_4Ti_5O_{12}$ coating layers of LT2-LCO$_{Mg}$ and LT2-LCO were compared. Fig. 7 shows enlarged HAADF STEM images, which were viewed along the [1 1 0] direction, of the two samples. In Fig. 7a, the different atomic columns of $Li_4Ti_5O_{12}$ in the charged state of LT2-LCO (without Mg doping) are revealed based on the contrast, where the 16d Ti sites are clearly identified as shown in the contrast line profile. The strong and weak spots indicate that there are two different Ti columns (Ti$_a$ and Ti$_b$ in Fig. 7a) and the population of Ti in the Ti$_a$ columns is greater than that in the Ti$_b$ columns. This observation on spinel $Li_4Ti_5O_{12}$ by STEM was previously reported by Lu et al. [41]. and is reproduced here. In their study, the 8a Li sites were also successfully visualized using the ABF images, which is not possible by the HAADF images due to the low atomic number of Li ions. Meanwhile, a notable change in the contrast was observed in the $Li_4Ti_5O_{12}$ coating layer of the Mg-doped sample (LT2-LCO$_{Mg}$). As shown in Fig. 7b, bright white spots are appeared in the centers of diamond patterns of Ti ions. The new spots obviously come from the Mg ions. It is considered that the excellent electrochemical performances of LT2-LCO$_{Mg}$ are originated by the high electrical conductivity of Mg-doped $Li_4Ti_5O_{12}$. Chen et al. reported that the Mg-doped $Li_4Ti_5O_{12}$ exhibits a completely different electrical behavior ($\sigma = 10^{-2}$ S cm^{-1}) from the nearly insulating undoped $Li_4Ti_5O_{12}$ [19]. The current-voltage (IV) curves in Fig. 8 provide supporting evidences of these different electrical characteristics. In this experiment, one probe contacts the active materials of $LiCoO_2$ while the other probe is placed on the $Li_4Ti_5O_{12}$ coating layer as demonstrated in the figure inset. Because the fully lithiated $LiCoO_2$ is an insulator [42], the current at the discharged state of LT2-LCO$_{Mg}$ is almost zero. Meanwhile, the significant current is detected at its charged state, which indicates that both the delithiated $LiCoO_2$ and Mg-doped $Li_4Ti_5O_{12}$ are electrically conductive. However, the conductivity of the coating layer of LT2-LCO, that is, the undoped $Li_4Ti_5O_{12}$, is not as good as that of the Mg-doped $Li_4Ti_5O_{12}$. Hence, the formation of a conductive coating material, that is, Mg-doped $Li_4Ti_5O_{12}$, is an

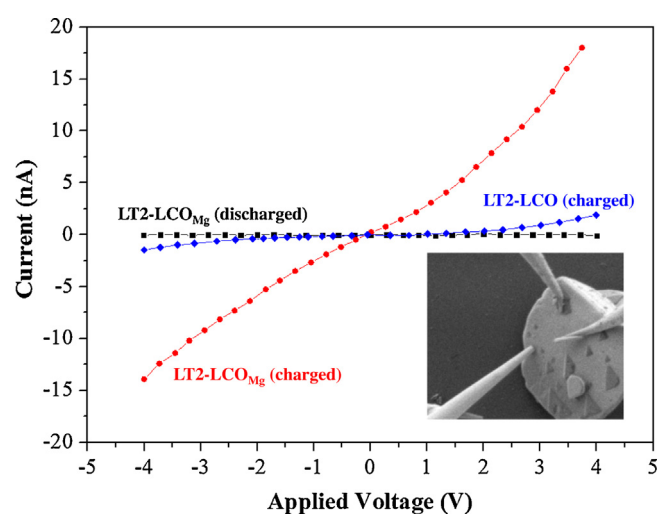

Fig. 8. Current-voltage plot of discharged/charged LT2-LCO$_{Mg}$ and charged LT2-LCO. The inset is an SEM image of measuring by nano probe.

origin of synergistic effects of coating and doping for the cathode materials in this study.

4. Conclusion

We synthesized and characterized lithium titanate-coated $LiCoO_2$ with Mg doping in which the remaining lithium carbonates after synthesis of the active materials were reused as a lithium source for the coating materials. Due to its excellent stability during charging/discharging, the spinel $Li_4Ti_5O_{12}$, which was obtained from the high concentration of Ti source, showed much better electrochemical performances as a coating material than the monoclinic Li_2TiO_3, which was from the low concentration of Ti source. In addition, it was observed that the dopant ions (Mg^{2+}) in the active materials diffused to the coating layer, and efficiently improved the cell performances by formation of highly conductive Mg-doped $Li_4Ti_5O_{12}$, which is considered as a mechanism of synergistic effects of coating and doping for the cathode materials in LIB.

Appendix A. Supplementary data

Supplementary data associated with this article can be found, in the online version, at http://dx.doi.org/10.1016/j.electacta.2015.10.135.

References

[1] J. Vetter, P. Novák, M.R. Wagner, C. Veit, K.-C. Möller, J.O. Besenhard, M. Winter, M. Wohlfahrt-Mehrens, C. Vogler, A. Hammouche, J. Power Sources 147 (2005) 269–281.
[2] M.M. Thackeray, J. Electrochem. Soc. 142 (1995) 2558–2563.
[3] G. Ceder, M.K. Aydinol, Solid State Ionics 109 (1998) 151–157.
[4] P. Arora, R.E. White, M. Doyle, J. Electrochem. Soc. 145 (1998) 3647–3667.
[5] Z. Chen, Y. Qin, K. Amine, Y.-K. Sun, J. Mater. Chem. 20 (2010) 7606–7612.
[6] J. Lu, Q. Peng, W. Wang, C. Nan, L. Li, Y. Li, J. Am. Chem. Soc. 135 (2013) 1649–1652.
[7] H. Deng, P. Nie, H. Luo, Y. Zhang, J. Wang, X. Zhang, J. Mater. Chem. A 2 (2014) 18256–18262.
[8] E. Ferg, R.J. Gummow, A. Dekock, M.M. Thackeray, J. Electrochem. Soc. 141 (1994) L147–L150.
[9] T. Ohzuku, A. Ueda, N. Yamamoto, J. Electrochem. Soc. 142 (1995) 1431–1435.
[10] C.P. Sandhya, B. John, C. Couri, Ionics 20 (2014) 601–620 and references therein.
[11] D.-Q. Liu, X.Q. Liu, Z.-Z. He, Mater. Chem. Phys. 105 (2007) 362–366.
[12] T.-F. Yi, J. Shu, Y.-R. Zhu, A.-N. Zhu, R.-S. Zhu, Electrochem. Commun. 11 (2009) 91–94.
[13] Y.-R. Zhu, T.-F. Yi, R.-S. Zhu, A.-N. Zhou, Ceram. Int. 39 (2013) 3087–3094.
[14] J. Li, Y. Zhu, L. Wang, C. Cao, ACS Appl. Mater. Interfaces 6 (2014) 18742–18750.
[15] N. Ohta, K. Takada, L. Zhang, R. Ma, M. Osada, T. Sasaki, Adv. Mater. 18 (2006) 2226–2229.
[16] T.-F. Yi, J. Shu, C.-B. Yue, X.-D. Zhu, A.-N. Zhou, Y.-R. Zhu, R.-S. Zhu, Mater. Res. Bull. 45 (2010) 456–459.
[17] T.-F. Yi, J. Shu, Y. Wang, J. Xue, J. Meng, C.-B. Yue, R.-S. Zhu, Surf. Coat. Tech. 205 (2011) 3885–3889.
[18] G.T.-K. Fey, C.-F. Huang, P. Muralidharan, E.S.-S. Chang, J. Power Sources 174 (2007) 1147–1151.
[19] C.H. Chen, J.T. Vaughey, A.N. Jansen, D.W. Dees, J. Electrochem. Soc. 148 (2001) A102–A104.
[20] S. Levasseur, M. Menetrier, C. Delmas, Chem. Mater. 14 (2002) 3584–3590.
[21] H.-J. Kim, Y.U. Jeong, J.-H. Lee, J.-J. Kim, J. Power Sources 159 (2006) 233–236.
[22] H. Tukamoto, A.R. West, J. Electrochem. Soc. 144 (1997) 3164–3168.
[23] F. Nobili, S. Dsoke, F. Croce, R. Marassi, Electrochim. Acta 50 (2005) 2307–2313.
[24] F. Nobili, F. Croce, R. Tossici, I. Meschini, P. Reale, R. Marassi, J. Power Sources 197 (2012) 276–284.
[25] F. Zhou, W. Luo, X. Zhao, J.R. Dahn, J. Electrochem. Soc. 156 (2009) A917–A920.
[26] H.-S. Kim, T.-K. Ko, B.-K. Na, W.I. Cho, B.W. Chao, J. Power Sources 138 (2004) 232–239.
[27] S. Valanarasu, R. Chandramohan, Cryst. Res. Technol. 45 (2010) 835–839.
[28] R. Alcántara, P. Lavela, J.L. Tirado, R. Stoyanova, E. Zhecheva, J. Solid State Chem. 134 (1997) 265–273.
[29] M. Zhou, M. Yoshio, S. Gopukumar, J. Yamaki, Chem. Mater. 15 (2003) 4699–4702.
[30] M.-H. Park, M. Noh, S. Lee, M. Ko, S. Chae, S. Sim, S. Choi, H. Kim, H. Nam, S. Park, J. Cho, Nano Lett. 14 (2014) 4083–4089.
[31] M. Mladenov, R. Stoyanova, E. Zhecheva, S. Vassilev, Electrochem. Commun. 3 (2001) 410–416.
[32] Z. Wang, L. Liu, L. Chen, X. Huang, Solid State Ionics 148 (2002) 335–342.
[33] H. Zhao, L. Gao, W. Qui, X. Zhang, J. Power Sources 132 (2004) 195–200.
[34] J.-H. Shim, S. Lee, S.S. Park, Chem. Mater. 26 (2014) 2537–2543.
[35] S.D. Findlay, N. Shibata, H. Sawada, E. Okunishi, Y. Kondo, T. Yamamoto, Y. Ikuhaha, Appl. Phys. Lett. 95 (2009) 191913.
[36] G. Izquierdo, A.R. West, Mater. Res. Bull. 15 (1980) 1655–1660.
[37] S. Takai, M. Kamata, S. Fujine, K. Yoneda, K. Kanda, T. Esaka, Solid State Ionics 123 (1999) 165–172.
[38] B. Ruprecht, M. Wilkening, R. Uecker, P. Heitjans, Phys. Chem. Chem. Phys. 14 (2012) 11974–11980.
[39] N.V. Tarakina, R.B. Neder, T.A. Denisova, L.G. Maksimova, Y.V. Baklanova, A.P. Tyutyunnik, V.G. Zubkov, Dalton Trans. 39 (2010) 8168–8176.
[40] P. He, H. Yu, D. Li, H. Zhou, J. Mater. Chem. 22 (2012) .
[41] X. Lu, L. Zhao, X. He, R. Xiao, L. Gu, Y.-S. Hu, H. Li, Z. Wang, X. Duan, L. Chen, J. Maier, Y. Ikuhara, Adv. Mater. 24 (2012) 3233–3238.
[42] F. Sauvage, J.-M. Tarascon, E. Baudrin, J. Phys. Chem. C 111 (2007) 9624–9630.